Published in final edited form as:
Nucl Med Biol. 2013 May ; 40(4): 524–528. doi:10.1016/j.nucmedbio.2013.01.008.

Antilipolytic drug boosts glucose metabolism in prostate cancer☆

Kim Francis Andersen[a,*], **Vadim Divilov**[b], **Jacek Koziorowski**[a], **NagaVaraKishore Pillarsetty**[b], and **Jason S. Lewis**[b]

[a]Department of Clinical Physiology & Nuclear Medicine, Herlev Hospital, University Hospital of Copenhagen, Herlev, Denmark

[b]Radiochemistry and Imaging Sciences Services, Department of Radiology, Memorial Sloan-Kettering Cancer Center, New York, NY, USA

Abstract

Introduction—The antilipolytic drug Acipimox reduces free fatty acid (FFA) levels in the blood stream. We examined the effect of reduced FFAs on glucose metabolism in androgen-dependent (CWR22R*v*1) and androgen-independent (PC3) prostate cancer (PCa) xenografts.

Methods—Subcutaneous tumors were produced in nude mice by injection of PC3 and CWR22R*v*1 PCa cells. The mice were divided into two groups (Acipimox vs. controls). Acipimox (50 mg/kg) was administered by oral gavage 1 h before injection of tracers. 1 h after i.v. co-injection of 8.2 MBq (222±6.0 μCi) ^{18} F-FDG and~0.0037 MBq (0.1 μCi) ^{14}C-acetate, ^{18} F-FDG imaging was performed using a small-animal PET scanner. Counting rates in reconstructed images were converted to activity concentrations. Quantification was obtained by region-of-interest analysis using dedicated software. The mice were euthanized, and blood samples and organs were harvested. ^{18} F radioactivity was measured in a calibrated γ-counter using a dynamic counting window and decay correction. ^{14}C radioactivity was determined by liquid scintillation counting using external standard quench corrections. Counts were converted into activity, and percentage of the injected dose per gram (%ID/g) tissue was calculated.

Results—FDG biodistribution data in mice with PC3 xenografts demonstrated doubled average %ID/g tumor tissue after administration of Acipimox compared to controls (7.21±1.93 vs. 3.59±1.35, P=0.02). Tumor-to-organ ratios were generally higher in mice treated with Acipimox. This was supported by PET imaging data, both semi-quantitatively (mean tumor FDG uptake) and visually (tumor-to-background ratios). In mice with CWR22R*v*1 xenografts there was no effect of Acipimox on FDG uptake, either in biodistribution or PET imaging. ^{14}C-acetate uptake was unaffected in PC3 and CWR22R*v*1 xenografts.

Conclusions—In mice with PC3 PCa xenografts, acute administration of Acipimox increases tumor uptake of ^{18} F-FDG with general improvements in tumor-to-background ratios. Data indicate that administration of Acipimox prior to ^{18} F-FDG PET scans has potential to improve sensitivity and specificity in patients with castration-resistant advanced PCa.

☆Conflict of interest: The authors declare that they have no conflict of interest.

*Corresponding author. Department of Clinical Physiology, Nuclear Medicine & PET, Rigshospitalet, University Hospital of Copenhagen, Blegdamvej 9, DK-2100 Copenhagen, Denmark. Tel.: +45 35457068; fax: +45 35453898. dr.kimfandersen@hotmail.com. .

Keywords

Acipimox; Free fatty acid; ^{18} F-FDG; Glucose; Metabolism; Prostate cancer

1. Introduction

1.1. Tumor energy metabolism

In general, glucose appears to be the most important energy substrate for tumors. Under normoxic conditions glucose is preferentially metabolized by the tricarboxylic acid (TCA) cycle and electron transport chain (oxidative phosphorylation), while under hypoxic conditions the glycolytic pathway is used. Despite the efficiency of the TCA cycle and electron transport chain to produce adenosine 5′-triphosphate (ATP) from glucose, some tumor cells continue to use glycolysis for ATP production in the presence of oxygen, also known as the Warburg effect [1]. Additionally, Herbert Crabtree observed an inhibition of oxygen consumption by adding glucose to microorganisms that have a high rate of aerobic glycolysis, which also occurs in most malignancies (the Crabtree effect) [2]. Summarized, both the Warburg and Crabtree effects suggest that an altered metabolic control and/or enzymes play a role in tumor glucose metabolism. However, tumors can also use other energy substrates, including fatty acids, which are the most reduced energy substrate available to cells. They provide the most ATP when metabolized, although their metabolism is oxygen dependent. There are two sources of fatty acids for tumors; free fatty acids and endogenous lipid esters from both tumor and normal tissues.

1.2. Interaction between tumor glucose and fatty acid metabolism

The interaction between glucose and free fatty acids (FFAs) metabolism was first demonstrated in a perfused rat heart [3]. Thereafter the glucose–FFA cycle has been shown to be operational in the human heart [4,5], skeletal muscles [6], as well as at whole body level [7]. Although several enzymes are involved in glycolysis, only a few key enzymes regulate the glucose flux. Phosphofructokinase is an enzyme that controls partially the selection of fuels. The activity of phosphofructokinase is inhibited by excess of citrate and ATP produced by metabolism of FFA and lactate. This leads to accumulation of glucose 6-phosphate, which restrains further uptake and phosphorylation of glucose by allosteric inhibition of hexokinase [8]. Conversely, when citrate and ATP levels are decreased, the inhibitory effects are reduced and the activity of phosphofructokinase increases, leading to increased glucose transport and phosphorylation. While the function of the glucose–FFA cycle has been well established in normal tissues and healthy subjects, the picture is different in cancer patients who show tumor-associated changes in host metabolism.

1.3. Effects of the antilipolytic drug Acipimox

Acipimox is a long-acting ($t_{½plasma}$~2 h) nicotinic acid derivative, which through its antilipolytic actions is used to inhibit the release of non-esterified fatty acids from adipose tissue and reduce total serum triglyceride and cholesterol levels. Administration of Acipimox has no effect on whole body glucose utilization after an overnight fast [9]. This does not preclude redistribution of glucose uptake between tissues or a change in the fate of glucose. In keeping with the latter alternative, Acipimox enhances glucose and decreases lipid oxidation. Acipimox also decreases glucose utilization for gluconeogenesis, which might in part explain why total glucose utilization remains unchanged although glucose oxidation increases [9].

1.4. Nuclear medicine imaging of glucose metabolism in prostate cancer

Prostate cancer is the most common malignancy among men in the United States, accounting for approximately one third of all cancer diagnoses. It is estimated that 240,890 men will be diagnosed with and 33,720 men will die of cancer of the prostate in 2011 [10]. Prostate cancers vary widely in their rate of growth, aggressiveness, and tendency to metastasize. The biology of this disease evolves from a small, slow-growing, androgen-dependent 'indolent' carcinoma toward a more and more aggressive, androgen-independent tumor during the course of progression [11,12]. Among the currently available nuclear medicine imaging modalities positron emission tomography (PET) offers several advantages compared to single-photon emission computed tomography (SPECT), especially in terms of spatial resolution and acquisition time (whole-body imaging in three dimensions in a relatively short amount of time). This has resulted in a clear tendency of development and application of PET agents in a number of clinical settings (diagnosis, staging, treatment evaluation). PET imaging with the glucose analogue 18-fluorine fluoro-2-deoxy-D-glucose (^{18} F-FDG) takes advantage of the increase in glycolytic flux in cancer. Unfortunately, a fraction of prostate cancers possesses a relatively slow metabolic rate and expresses fewer GLUT-1 binding sites (a hexose transporter), leading to lower FDG uptake compared with other cancers.

The results of prostate cancer PET imaging with ^{18} F-FDG are in general disappointing [13–17]. Despite its poor reputation from earlier reports, ^{18} F-FDG is in fact not an unsuitable tracer for the investigation of prostate carcinoma, but at present needs to be used in carefully selected groups of patients [18–22]. The effect of Acipimox on fatty acid and glucose metabolism in malignant prostate cells has not been investigated — we hypothesize that Acipimox through its antilipolytic effect may increase FDG tumor uptake in prostate cancer xenografts. Consequently, the diagnostic properties of ^{18} F-FDG PET regarding different clinical settings in patients with prostate cancer may be improved.

2. Methods

2.1. Generation of tumor xenografts

All animal experiments were conducted in accordance with protocols approved by the Institutional Animal Care and Use Committee of Memorial Sloan-Kettering Cancer Center and followed National Institutes of Health guidelines for animal welfare. Tumor cell lines were obtained from the American Type Culture Collection and cultured under conditions provided by the supplier. The cell lines included PC3 (derived from androgen independent prostate cancer bone metastasis) and CWR22Rv1 (derived from a more androgen dependent prostate cancer primary tumor). Subcutaneous tumors were produced on the right shoulder of nude mice (20–25 g; Taconic) by subcutaneous injection of tumor cells (PC3: 5×10^6 cells, n=10; CWR22Rv1: 10×10^6 cells, n=10) in 200 μL consisting of 100 μL of cell culture medium and 100 μL of Matrigel (BD Biosciences) under 2% isoflurane anesthesia.

2.2. Small-animal PET

The mice were divided into two groups (Acipimox (n=5 for each xenograft) vs. control (n=5 for each xenograft)). Acipimox (50 mg/kg) was administered to the mice using the oral gavage technique 1 h before injection of the tracers [23]. Imaging was performed by use of a dedicated high-resolution small-animal PET scanner (microPET R4 Rodent; Concorde Microsystems Inc., Knoxville, TN, USA). The mice were maintained under 2% isoflurane anesthesia in oxygen at 2 L/min during the entire scanning period. Imaging was performed 1 h after co-injection of 8.2 MBq (222 μCi±6.0 μCi) ^{18} F-FDG and~0.0037 MBq (0.1 μCi) ^{14}C-1-acetate (^{14}C-acetate) via the tail vein. An energy window of 350–700 keV and a coincidence timing window of 6 ns were used. The image data were corrected for non-

uniformity of the scanner response, dead-time count losses, and physical decay to the time of injection. No correction was applied for attenuation, scatter, or partial-volume averaging. The measured reconstructed spatial resolution of the R4 microPET scanner is approximately 2.0 mm in full width at half maximum at the center of the field of view. The counting rates in the reconstructed images were converted to activity concentrations (percentage injected dose [%ID] per gram of tissue) by use of a system calibration factor derived from the imaging of a mouse-sized water equivalent phantom containing ^{18} F. Quantification was obtained by region-of-interest analysis using ASIPro VM software (v. 6.3.3.0, Concorde Microsystems Inc., Knoxville, TN, USA).

2.3. In vivo biodistribution studies

Immediately after PET imaging the mice were euthanized and then blood samples and organs were harvested. ^{18} F radioactivity was measured in a calibrated γ-counter (2480 Wizard^2 Automatic Gamma Counter; PerkinElmer, Inc.) using a dynamic counting window (peak 511 keV; threshold 20%) and decay correction. For measuring ^{14}C activity, all samples were solubilized (Soluene-350; Packard Instrument Co., Inc.) after the ^{18} F radioactivity counting. The samples were then stored at 4 °C for 2 days to allow for ^{18} F decay. A scintillant agent (Insta-Fluor; Packard Instrument Co., Inc.) was added to solubilized samples, and ^{14}C radioactivity was determined by liquid scintillation counting (Tri-Carb Liquid Scintillation Analyzer 1600TR; Packard Instrument Co., Inc.) using external standard quench corrections. The counts were converted into activity, and %ID/g was calculated by dividing by decay-corrected injected activity and the weight of the organ.

The Student t-test was made using IBM® SPSS® Statistics 19.0 (SPSS Inc., IBM, Somers, NY, USA). All P-values were calculated as two-sided and differences were considered significant at $P<0.05$.

3. Results

3.1. Small-animal PET

Maximal and mean tumor uptakes of FDG in the different prostate cancer xenografts are summarized in Table 1. In PC3 xenografts FDG uptake generally was higher in mice treated with Acipimox than in controls, and even though no significant P-values were demonstrated, there was a clear tendency towards an effect of Acipimox, especially in mean tumor FDG uptake (P=0.08). Additionally, when assessing the reconstructed PET images visually, tumor-to-background ratios were slightly better in mice treated with Acipimox. No significant differences in FDG uptake were demonstrated in mice with CWR22R*v*1 xenografts.

3.2. In vivo biodistribution

FDG biodistribution data in mice with PC3 xenografts (Table 2) demonstrated twice as high average %ID/g tumor tissue after a single administration of Acipimox compared to the control group (7.21±1.93 vs. 3.59±1.35, P=0.02). Tumor-to-organ ratios were generally higher in mice treated with Acipimox, especially when comparing tumor uptake of FDG with uptake in blood, liver, muscle, and bone tissue (Table 2 and Fig. 1). However, in mice with CWR22R*v*1 xenografts there was no effect of Acipimox on FDG uptake (Table 3). ^{14}C-acetate uptake was unaffected by administration of Acipimox in both PC3 and CWR22R*v*1 xenografts.

4. Discussion

This is the first study demonstrating a positive effect of the antilipolytic drug Acipimox on tumor FDG uptake in mice with the androgen independent prostate cancer xenograft PC3. The results are in contrast to reports by Nuutinen et al. [24], where no significant alterations in ^{18} F-FDG uptake on PET in patients with malignant lymphoma were demonstrated. However, the patients in that study were inhomogeneous in terms of lymphoma subtype, and the number of included study objects was low (n=11). Furthermore, administration of Acipimox has no effect on whole body glucose utilization after an overnight fast [9], but this does not preclude redistribution of glucose uptake between tissues [6] or even a change in the fate of glucose. Both the Warburg and Crabtree effects suggest that an altered metabolic control and/or enzymes play a role in tumor glucose metabolism, and possible causes of the Warburg effect include: 1) changes in characteristics or amounts of glucose transporters, 2) changes in characteristics or amounts of isoenzymes caused by neoplastic transformation (e.g. hexokinase, lactate dehydrogenase), and/or 3) impaired function of cytosolic/mitochondrial redox shuttle systems [25]. Our data support that a metabolic switch in this specific prostate cancer xenograft (PC3) in terms of preferred energy substrate can be induced by antilipolysis. However, further studies on the antilipolytic effect on the glucose-FFA cycle in different prostate cancer cell lines are needed to explore the subject.

Despite its poor reputation, prostate cancer PET imaging with ^{18} F-FDG has demonstrated significant value in a number of circumstances, that being diagnosis and staging in primary tumors with known or suspected high Gleason score (grade of differentiation), assessing the extent of advanced disease when biochemical relapse (increasing PSA levels) occurs, assessing the extent of metabolic active castration resistant disease, response evaluation of anti-androgen treatment, as well as tumor ^{18} F-FDG uptake on PET images being an independent prognostic factor [18–22]. Careful selection is essential before performing ^{18} F-FDG PET imaging in this group of patients, which is being understated by our study, as biodistribution demonstrated that FDG uptake in the androgen independent prostate cancer xenograft PC3 was improved after acute administration of the antilipolytic drug Acipimox, while FDG uptake in the more androgen dependent xenograft CWR22R*v*1 was unaffected.

The generally disappointing results of prostate cancer PET imaging with ^{18} F-FDG are likely to be related to four factors [26]: 1) A relatively lower metabolic rate in the majority of prostate cancers with lower ^{18} F-FDG uptake, 2) Older image reconstruction techniques (i.e., use of filtered back projection instead of iterative reconstruction), 3) Location of the prostate adjacent to the urinary bladder, and 4) The lack of appropriate patient selection. However, it is important to not forget the heterogeneous nature and the potential indolent course of this disease, with bone metastases being one of the main manifestations in castration-resistant advanced prostate cancer. The differences observed between PC3 and CWR22R*v*1 xenografts in this study regarding tumor FDG uptake and tumor-to-background ratios in mice are probably a result of this heterogeneity, as PC3 xenografts are less androgen-dependent and consequently have a more aggressive nature than CWR22R*v*1 xenografts. Theoretically, a higher tumor uptake of the tracer and especially an improved tumor-to-background ratio in patients with aggressive (i.e. less androgen-dependent) prostate cancer could help distinguishing between benign (degenerative, sclerotic lesions) and malignant manifestations (sclerotic metastases) in bone tissue, which is the most common location for metastatic disease in prostate cancer. With a huge difference in the therapy regimen chosen depending on the prostate cancer being locoregional or advanced, the importance of getting a precise assessment of disease extent is crucial.

Possible misinterpretations of the results could be related to the fact that the rate of phosphorylation in tumors can be altered. Kaarstad and co-workers [27] demonstrated –

besides ^{18} F-FDG-6-phosphate (P) – the formation of two secondary metabolites to ^{18} F-FDG-6-P (^{18} F-FD-PG1 and ^{18} F-FDG-1,6-P_2) in malignant tumor tissue after ^{18} F-FDG administration. However, they did not identify any of the nucleotide derivatives of ^{18} F-FDG-1-P or incorporation of ^{18} F-FDG into glycogen. The fact that ^{18} F-FDG-metabolites other than ^{18} F-FDG-6-P were found in tumor tissue may have implications for the interpretation of estimated kinetic rate constants in terms of the enzymatic processes. However, the finding does not in any way alter the conventional use of ^{18} F-FDG uptake in tumor tissue as an indicator of the rate of glucose use, because the trapped label in tissue still reflects the ^{18} F-FDG phosphorylation rate regardless of whether the label is associated with ^{18} F-FDG-6-P or with the products of ^{18} F-FDG-6-P. It would have been a completely different story if the discovered metabolites were products of ^{18} F-FDG directly, that is, in parallel or in competition with the phosphorylation reaction. Additionally, time course studies of percentage tissue content of FDG-6-P and its secondary metabolites in mice bearing different carcinomas were relatively consistent from approximately 30 min and thereafter, justifying the imaging time points chosen in our study (images acquired approximately 60 min p.i.).

Common side effects to acute administration of Acipimox are flushing and headaches. These potential side effects in humans can be extensively reduced by administration of aspirin 20–30 min prior to administration of Acipimox. Consequently, there should be no concerns regarding that the clinical impact of the effect of Acipimox on tumor FDG uptake and tumor-to-background ratios could be balanced by the potential side effects of the drug.

The exact clinical impact in humans of a slightly larger tumor uptake of FDG or significantly higher tumor-to-background ratios after administration of Acipimox both in terms of diagnosing primary prostate cancer and/or metastatic disease is yet to be examined. However, as PC3 xenograft FDG uptake and tumor-to-background ratios were improved after administration of the antilipolytic drug Acipimox, we conclude that administration of this drug prior to a FDG-PET scan has potential to improve the diagnostic properties in patients with castration resistant advanced prostate cancer.

Acknowledgments

Technical services were provided by the MSKCC Small-Animal Imaging Core Facility, supported in part by NIH Small-Animal Imaging Research Program (SAIRP) grant R24 CA83084. Support from the MSKCC Radiochemistry and Cyclotron Core for production and supply of ^{18} F-FDG is also acknowledged.

References

[1]. Warburg, O. Stoffweschel der Tumoren. Verlag Springer; Berlin: 1926.

[2]. Crabtree HG. Observations on the carbohydrate metabolism of tumours. Biochem J. 1929; 23(3): 536–45. [PubMed: 16744238]

[3]. Randle PJ, Garland PB, Hales CN, Newsholme EA. The glucose fatty-acid cycle. Its role in insulin sensitivity and the metabolic disturbances of diabetes mellitus. Lancet. 1963; 13(7285):785–9. 1. [PubMed: 13990765]

[4]. Knuuti MJ, Maki M, Yki-Jarvinen H, Voipio-Pulkki LM, Harkonen R, Haaparanta M, et al. The effect of insulin and FFA on myocardial glucose uptake. J Mol Cell Cardiol. 1995; 27(7):1359–67. [PubMed: 7473782]

[5]. Nuutila P, Koivisto VA, Knuuti J, Ruotsalainen U, Teras M, Haaparanta M, et al. Glucose–free fatty acid cycle operates in human heart and skeletal muscle in vivo. J Clin Invest. 1992; 89(6): 1767–74. [PubMed: 1601987]

[6]. Nuutila P, Knuuti MJ, Raitakari M, Ruotsalainen U, Teras M, Voipio-Pulkki LM, et al. Effect of antilipolysis on heart and skeletal muscle glucose uptake in overnight fasted humans. Am J Physiol. 1994; 267(6 Pt 1):E941–6. [PubMed: 7810638]

[7]. Thiebaud D, DeFronzo RA, Jacot E, Golay A, Acheson K, Maeder E, et al. Effect of long chain triglyceride infusion on glucose metabolism in man. Metabolism. 1982; 31(11):1128–36. [PubMed: 6752642]

[8]. Randle PJ, Newsholme EA, Garland PB. Regulation of glucose uptake by muscle. 8. Effects of fatty acids, ketone bodies and pyruvate, and of alloxan-diabetes and starvation, on the uptake and metabolic fate of glucose in rat heart and diaphragm muscles. Biochem J. 1964; 93(3):652–65. [PubMed: 4220952]

[9]. Puhakainen I, Yki-Jarvinen H. Inhibition of lipolysis decreases lipid oxidation and gluconeogenesis from lactate but not fasting hyperglycemia or total hepatic glucose production in NIDDM. Diabetes. 1993; 42(12):1694–9. [PubMed: 8243814]

[10]. US National Cancer Institute. SEER database. 2012. Ref Type: Online Source

[11]. Chen CD, Welsbie DS, Tran C, Baek SH, Chen R, Vessella R, et al. Molecular determinants of resistance to antiandrogen therapy. Nat Med. 2004; 10(1):33–9. [PubMed: 14702632]

[12]. Craft N, Chhor C, Tran C, Belldegrun A, DeKernion J, Witte ON, et al. Evidence for clonal outgrowth of androgen-independent prostate cancer cells from androgen-dependent tumors through a two-step process. Cancer Res. 1999; 59(19):5030–6. [PubMed: 10519419]

[13]. Effert PJ, Bares R, Handt S, Wolff JM, Bull U, Jakse G. Metabolic imaging of untreated prostate cancer by positron emission tomography with 18fluorine-labeled deoxyglucose. J Urol. 1996; 155(3):994–8. [PubMed: 8583625]

[14]. Hofer C, Laubenbacher C, Block T, Breul J, Hartung R, Schwaiger M. Fluorine-18-fluorodeoxyglucose positron emission tomography is useless for the detection of local recurrence after radical prostatectomy. Eur Urol. 1999; 36(1):31–5. [PubMed: 10364652]

[15]. Liu IJ, Zafar MB, Lai YH, Segall GM, Terris MK. Fluorodeoxyglucose positron emission tomography studies in diagnosis and staging of clinically organ-confined prostate cancer. Urology. 2001; 57(1):108–11. [PubMed: 11164153]

[16]. Melchior SW, Brown LG, Figg WD, Quinn JE, Santucci RA, Brunner J, et al. Effects of phenylbutyrate on proliferation and apoptosis in human prostate cancer cells in vitro and in vivo. Int J Oncol. 1999; 14(3):501–8. [PubMed: 10024683]

[17]. Oyama N, Akino H, Suzuki Y, Kanamaru H, Sadato N, Yonekura Y, et al. The increased accumulation of [18 F] fluorodeoxyglucose in untreated prostate cancer. Jpn J Clin Oncol. 1999; 29(12):623–9. [PubMed: 10721945]

[18]. Fricke E, Machtens S, Hofmann M, van den Hoff J, Bergh S, Brunkhorst T, et al. Positron emission tomography with 11C-acetate and 18 F-FDG in prostate cancer patients. Eur J Nucl Med Mol Imaging. 2003; 30(4):607–11. [PubMed: 12589476]

[19]. Herrmann K, Schoder H, Eberhard S. FDG PET for the detection of recurrent/metastatic prostate carcinoma in patients with rising PSA after radical prostatectomy. J Nucl Med. 2004; 45:359. Ref Type: Abstract.

[20]. Larson SM, Morris M, Gunther I, Beattie B, Humm JL, Akhurst TA, et al. Tumor localization of 16beta-18 F-fluoro-5alpha-dihydrotestosterone versus 18 F-FDG in patients with progressive, metastatic prostate cancer. J Nucl Med. 2004; 45(3):366–73. [PubMed: 15001675]

[21]. Morris MJ, Akhurst T, Osman I, Nunez R, Macapinlac H, Siedlecki K, et al. Fluorinated deoxyglucose positron emission tomography imaging in progressive metastatic prostate cancer. Urology. 2002; 59(6):913–8. [PubMed: 12031380]

[22]. Nunez R, Macapinlac HA, Yeung HW, Akhurst T, Cai S, Osman I, et al. Combined 18 F-FDG and 11C-methionine PET scans in patients with newly progressive metastatic prostate cancer. J Nucl Med. 2002; 43(1):46–55. [PubMed: 11801702]

[23]. Carballo-Jane E, Gerckens LS, Luell S, Parlapiano AS, Wolff M, Colletti SL, et al. Comparison of rat and dog models of vasodilatation and lipolysis for the calculation of a therapeutic index for GPR109A agonists. J Pharmacol Toxicol Methods. 2007; 56(3):308–16. [PubMed: 17643322]

[24]. Nuutinen J, Minn H, Bergman J, Haaparanta M, Ruotasalainen U, Laine H, et al. Uncoupling of fatty acid and glucose metabolism in malignant lymphoma: a PET study. Br J Cancer. 1999; 80(3–4):513–8. [PubMed: 10408861]

[25]. Medina MA, NuñezdeCastro I. Glutaminolysis and glycolysis interactions in proliferant cells. Int J Biochem. 1990; 22(7):681–3. [PubMed: 2205518]

[26]. Schoder H, Larson SM. Positron emission tomography for prostate, bladder, and renal cancer. Semin Nucl Med. 2004; 34(4):274–92. [PubMed: 15493005]

[27]. Kaarstad K, Bender D, Bentzen L, Munk OL, Keiding S. Metabolic fate of 18 F-FDG in mice bearing either SCCVII squamous cell carcinoma or C3H mammary carcinoma. J Nucl Med. 2002; 43(7):940–7. [PubMed: 12097467]

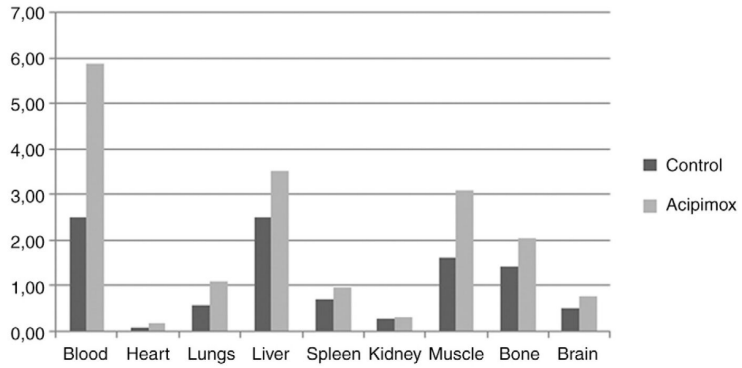

Fig. 1.
Tumor-to-organ ratios in terms of FDG uptake in mice with PC3 xenografts.

Table 1

Semi-quantitative tumor uptake of 18 F-FDG on microPET scans

PCa xenograft	Max uptake±SD (nCi/cc)	P	Mean uptake±SD (nCi/cc)	P
PC3 (n=10)				
Acipimox	5.207±1.03	0.18	4.188±1.06	0.08
Control	4.092±1.34		2.858±1.10	
CWR22Rv1 (n=10)				
Acipimox	8.930±2.69	0.82	6.521±1.83	0.59
Control	8.369±1.46		7.784±2.13	

Abbreviations: PCa: prostate cancer; SD: standard deviation.

Table 2

FDG biodistribution data in mice with PC3 xenografts

Organ	Avg. %ID/g±SD			Tumor/Organ	
	Control (n=5)	Acipimox (n=5)	P	Control	Acipimox
Tumor	3.59±1.35	7.21±1.93	0.02*	1.00	1.00
Blood	1.44±0.28	1.23±0.54	0.64	2.49	5.86
Heart	56.94±23.80	41.21±23.47	0.66	0.06	0.17
Lungs	6.42±2.73	6.69±1.07	0.68	0.56	1.08
Liver	1.43±0.42	2.06±0.69	0.16	2.51	3.50
Spleen	5.23±0.92	7.47±1.23	0.01*	0.69	0.97
Kidney	13.28±1.57	24.40±9.72	0.06	0.27	0.30
Muscle	2.21±0.72	2.34±1.32	0.55	1.62	3.08
Bone	2.56±1.10	3.54±1.40	0.30	1.40	2.04
Brain	7.07±1.15	9.55±3.17	0.19	0.51	0.75

Abbreviations: %ID/g: percentage of injected dose per gram; SD: standard deviation;

significant differences ($P<0.05$) marked with *.

Table 3

FDG biodistribution data in mice with CWR22Rv1 xenografts

Organ	Avg. %ID/g±SD			Tumor/Organ	
	Control (n=5)	Acipimox (n=5)	P	Control	Acipimox
Tumor	8.41±0.31	9.02±4.04	0.85	1.00	1.00
Blood	1.90±1.40	0.93±0.24	0.28	12.15	9.72
Heart	54.29±12.99	78.69±34.94	0.43	0.16	0.12
Lungs	7.40±0.16	12.15±3.99	0.21	1.14	0.74
Liver	1.58±0.05	4.36±2.62	0.21	5.33	2.07
Spleen	6.98±0.53	11.38±3.24	0.17	1.21	0.79
Kidney	21.42±8.81	23.79±7.48	0.77	0.39	0.38
Muscle	3.76±0.73	8.09±7.30	0.49	2.24	1.12
Bone	3.96±0.42	4.69±0.42	0.16	2.12	1.92
Brain	7.16±1.85	10.92±3.56	0.28	1.18	0.83

Abbreviations: %ID/g: percentage of injected dose per gram; SD: standard deviation.